Burning iron powder in a coal combustion chamber

R. Mehmood[1], S. Mehlhose[1*], Q. Fradet[1], S. Grusla[2], T. Zschunke[2], U. Riedel[1]

*sven.mehlhose@dlr.de

[1] *German Aerospace Center (DLR), Institute of Low-Carbon Industrial Processes, Äußere Oybiner Straße 14/16, 02763 Zittau, Germany*

[2] *Zittau/Görlitz University of Applied Sciences, Institute of Process Technology, Process Automation and Measurement Technology, Theodor-Körner-Allee 8, 02763 Zittau, Gemany*

Abstract

One of the greatest challenges of modernizing the energy supply is the need for large-scale seasonal energy storage. Renewable energy must be available in a form in which industry-relevant capacities can be stored over longer periods of time. Metal fuels can play a significant role here. In this concept, energy is released through the combustion of metal powder. To ensure climate neutrality, green hydrogen can be used to reduce the resulting metal oxides. Research and industry are investigating the possibility of commissioning power plants for iron combustion; we are also dedicating ourselves to this approach by investigating the retrofitting potential of existing coal-fired power plants.

The aim of this work is to obtain initial empirical evidence of the flame behaviour. The main question is the stabilization of the flame under varying operating conditions. For this purpose, we are using the MB1500 experimental combustion chamber designed for the investigation of pulverized lignite combustion, with a fuel heat output of up to 15 kW, which is hereby given a new application as the “Zittau Iron Combustion Chamber" (ZIICC). The ZIICC is a vertically aligned micro-combustion chamber that simulates the combustion behaviour of industrial combustion chambers. Firstly, the feasibility of iron powder combustion will be demonstrated by first mixing iron powder with pulverized lignite and then burning it in its pure form to generate a self-sustaining flame. Here, we will discuss the differences observed between pulverized lignite firing and iron powder combustion. Next, the oxygen content in the flue gas, or more specifically the associated feed mass flow of the iron powder, will be varied, generating primarily process and operational data. The differences in ignition behaviour between two different particle sizes will be investigated. Finally, we discuss the phenomenon of “fouling”, which has thus far only been observed in such bottom-up burners. The insights gained from these experiments will aid us in achieving our end goal of retrofitting coal-fired power plants to burn iron instead.

Introduction

As the date set by the German government for phasing out coal approaches, researchers are looking into what should happen to coal-fired power plants that are being decommissioned. To preserve as much of the infrastructure as possible, one option would be to convert the combustion chambers of such power stations from coal to another fuel. There are a number of CO_2-neutral options here, most of which involve various forms of biomass. Metal fuels are another upcoming alternative. These are based on the idea of releasing energy by burning metals and then reducing the resulting metal oxides using renewable energy to store energy in them again. Research in this area focuses on iron, which has proven to be a reliable energy source, with comparatively low combustion temperatures of iron, low NOx emissions from combustion and less nanoparticle formation compared to other metallic energy sources. The reduction of iron oxides is already being intensively investigated in the context of steel production, where iron ore is first reduced to pig iron and then processed into steel. On the other hand, there is a need for research into iron combustion to better understand the energy release step.

First, the individual combustion of particles has been examined closely. By igniting iron particles using focused lasers, it was determined, among other things, that particles ignite at temperatures between 1030 K and 1130 K and that larger particles have a higher probability of ignition [1]. Investigation using

tomographic methods [2] revealed the phase transitions of iron and iron oxide during combustion, as well as associated phenomena such as pore formation and the development of mixed phases. Laminar iron flames have also been investigated in various configurations. The combustion of iron under reduced gravity [3] shows that, in contrast to conventional fuels, iron can also exhibit discrete flames during combustion. Such flames are characterized by the need for a minimum flame temperature for their propagation. Iron flames in a laminar Bunsen burner [4] exhibit a flame velocity that is barely dependent on the equivalence ratio of the air-fuel mixture, in contrast to flames of other fuels.

Turbulent iron flames have so far been investigated predominantly in downward-facing configurations. The Metal Cyclonic Combustor (MC2) at Eindhoven University of Technology was developed to generate self-sustaining iron flames [5]. Furthermore, this burner was used to successfully demonstrate how NOx and nanoparticle formation can be prevented in iron flames [6]. Investigations of iron-methane flames in the 47 kWth laboratory burner at TU Darmstadt indicate the effects of preferential concentrations of iron [7]. In Canada, the first iron flames were generated in a converted fossil fuel burner by first generating an auxiliary flame from methane and then slowly reducing it. [8]. To the best of the authors' knowledge, the results presented here are the first from a floor burner that generates an upward-facing flame. First, the materials and methods used are described, starting with the Zittau Iron Combustion Chamber (ZIICC), the facility in which the experiments were conducted. The results of all experiments are then presented and interpreted.

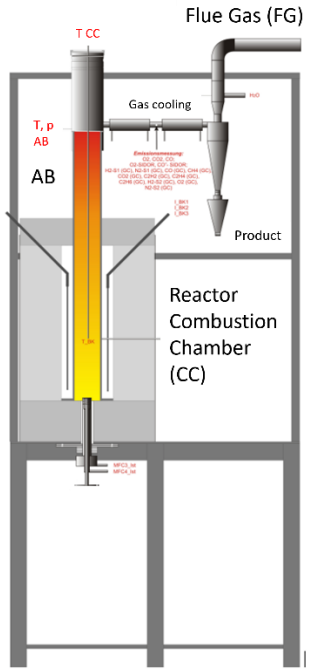

Burner Setup Parameters	
CC diameter	124 mm
CC height	750 mm
AB height	570 mm
Thermal Power	5 - 15 kW
Gas Residence Time	1.5 s
Max. Gas Velocity	1 m/s
Adjustable CC Temperature	800- 1500 °C
Adjustable AB Temperature	800 – 1100 °C

Figure 1. (left) Setup of the ZIICC. (right) Technical date and operation parameters of the ZIICC burner.

Materials and Methods

Figure 1 shows the structure of ZIICC. With a total height of 1720 mm, it is designed as a bottom-up burner with a vertical upward airflow. The fuel, in this case iron powder, is pneumatically conveyed from bottom to top through the combustion tube to the main outlet. The combustion tube also has a secondary outlet for air. The combustion chamber (CC), with an inner diameter of 124 mm and a height of 750 mm, is made of steel and equipped with an electric heater. Temperature sensors are located in the centre and on the wall. The afterburner chamber (AB) has a height of 570 mm. It contains both a temperature sensor and a pressure sensor, both located on the wall. It has an outlet pipe for the flue gases produced (FG) and solid product, in which both are cooled. This pipe contains the emission measurement systems (MRU gas analysis system, FTIR DX4000, Rosemount-SICK gas analysers). This

is followed by a cyclone separator to separate the flue gases from the solid product. The outlet for the flue gases includes a temperature sensor and measurement of the H_2O content.

Two types of iron powder were used for this experiment, which will be referred to as powder α and powder β. Powder α was purchased from the retailer 'Metallpulver24' (item p10-02977) and is said to have a purity of > 98% and an average diameter of < 30 µm. Powder β is an iron powder from Carl Roth (item 3718). According to the manufacturer's specifications, it has a purity of ≥ 99.5% and an average diameter of ~10 µm. Both types of powder are summarized in Table 1.

Table 1. Summary of the properties of the two iron powders used.

Powder	Supplier	Purity	Mean Diameter
α	Metallpulver24	> 98%	< 30 µm
β	Carl Roth	≥ 99.5%	10 µm

Results and Discussion

In the first series of experiments (DLR-001), the feasibility of iron powder combustion was investigated, initially using a mixture of 25% powder α and 75% lignite. After this mixture was combusted, an attempt was made to combust pure iron powder. This resulted in iron dust combustion with a self-sustaining flame; the heat release was sufficient to allow the external combustion chamber heating to be turned off. This demonstrates the feasibility of pure iron powder combustion. Almost all further test series were carried out with this powder; exceptions are indicated.
In the second series of experiments (DLR-002), the oxygen content in the exhaust gas was varied by changing the iron mass flow, as shown in Table 2.

Table 2. Operating parameters of the three experiments within the DLR-002 series of experiments. Here, the variation in oxygen content in the exhaust gas was investigated.

Experiment series	T CC in °C	T AB in °C	Vol% O_2 in Flue gas	Air volume flow in Nl/h	Fe mass flow in kg/h
DLR-002-001	1000	800	2.73	4048	4,65
DLR-002-002	1000	800	10	5765	1,92
DLR-002-003	1000	800	15	5764	1,28

Figure 2 shows the temperature of various parts of the combustion chamber. The temperature in the combustion chamber was always the highest, and the temperature of the wall was slightly higher than that in the afterburner chamber. This suggests that the heat release and thus the reaction mainly took place in the combustion chamber, but there was a strong enthalpy transport through the afterburner chamber. The temperature at the flue gas outlet was always between 200 °C and 300 °C despite the cooling being switched on, which is also due to this enthalpy flow. The cause of the enthalpy flow is discussed further below.

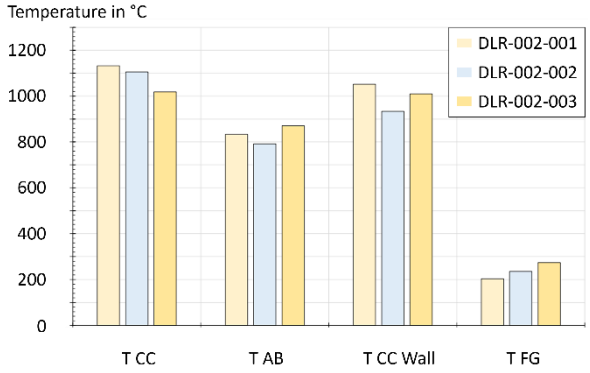

Figure 2. Time-averaged temperatures at various positions in the ZICC burner. TCC is the temperature in the combustion chamber, TAB in the afterburner chamber, TCC wall and TFG the temperatures of the combustion chamber walls and Flue gas respectively.

Figure 3 shows the gas concentrations of various exhaust gases measured at the flue gas outlet via FTIR on the left and the gas residence times for each experiment on the right, both in the combustion chamber and afterburner chamber, as well as in the entire reactor. The low concentrations of CO and CO_2 most likely stem from coal residues in the combustion chamber that were also burned. A small amount of water vapour was present, which probably originated from the residual moisture of the iron powder and the humidity of the air. The temperature of the combustion chamber rose with increasing residual oxygen content, while the temperatures in the afterburner chamber and on the combustion chamber wall reached a minimum at 10 vol% O_2. This was because the electric heating of the reactor was switched on during experiments DLR-002-001 and DLR-002-003. Due to the lower airflow rate in test DLR-002-001, the gas residence times for this test were longer than for tests DLR-002-002 and DLR-002-003.

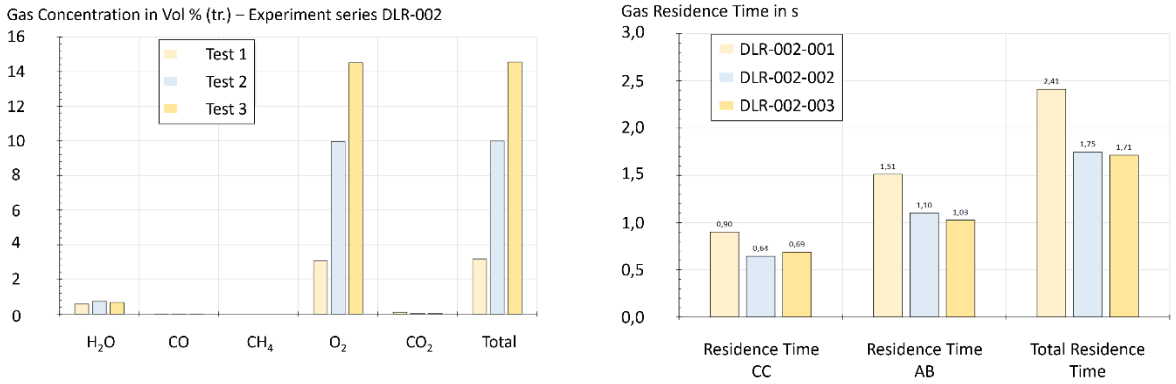

Figure 3. (left) Time-averaged gas concentrations of various exhaust gas species with varying oxygen content, measured at the flue gas outlet. (right) Residence times of the gas phase, both in the combustion chamber and afterburner chamber as well as overall, with varying oxygen content.

Figure 4 shows particle size distributions (PSDs) for both the starting material (blue) and the collected reaction product (red). It can be seen that the PSDs differ only slightly, which is because the iron powder remained predominantly in a condensed state during the reaction. This is advantageous for cyclic reaction control. In addition, the PSD of the reaction product deposited on the viewing window of the combustion chamber is shown (grey). Two peaks can be seen here: one at approx. 35 µm, which corresponds to the peaks of the other two PSDs, and one at approx. 2 µm. This is probably due to fine particles formed by micro-explosions.

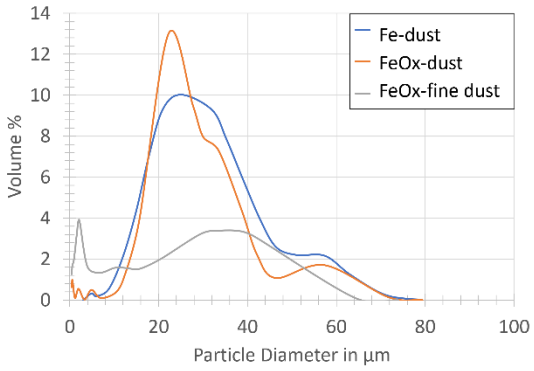

Figure 4. Particle size distributions for the experiment series DLR-002: Reactant powder ("Fe-dust", blue), reaction product collected after the cyclone ("FeOx-dust", orange), fine particles collecting at the viewing window of the reactor ("FeOx-fine dust", gray).

These fine particles were not observed in the product analysis, although they probably spread in all three spatial directions in the combustion chamber; it cannot be ruled out that they were contained in the flue gas. This would also explain the high temperatures in the afterburner chamber and, above all, in the flue

gas. Figure 5 shows images of the iron powder, both in its initial state (c) and after combustion in test DLR-002-002 (a) and test DLR-002-003 (b), taken using scanning electron microscopy (SEM). We see that the powder had irregular shapes before combustion, while it became spherical after combustion. The reason for this is the melting of the particles during the combustion process. All images show similar amounts of small particles despite different test conditions, indicating that the residual oxygen content had no influence on the formation of these particles. These particles are presumably the same ones that caused the 2 µm peak in Figure 4(c). In the image for experiment DLR-002-002, with 10 vol % O_2, a lamellar structure was observed on the iron surface, while at 15 vol % O_2, the iron surface exhibits a filamentous surface with areas that are oriented differently.

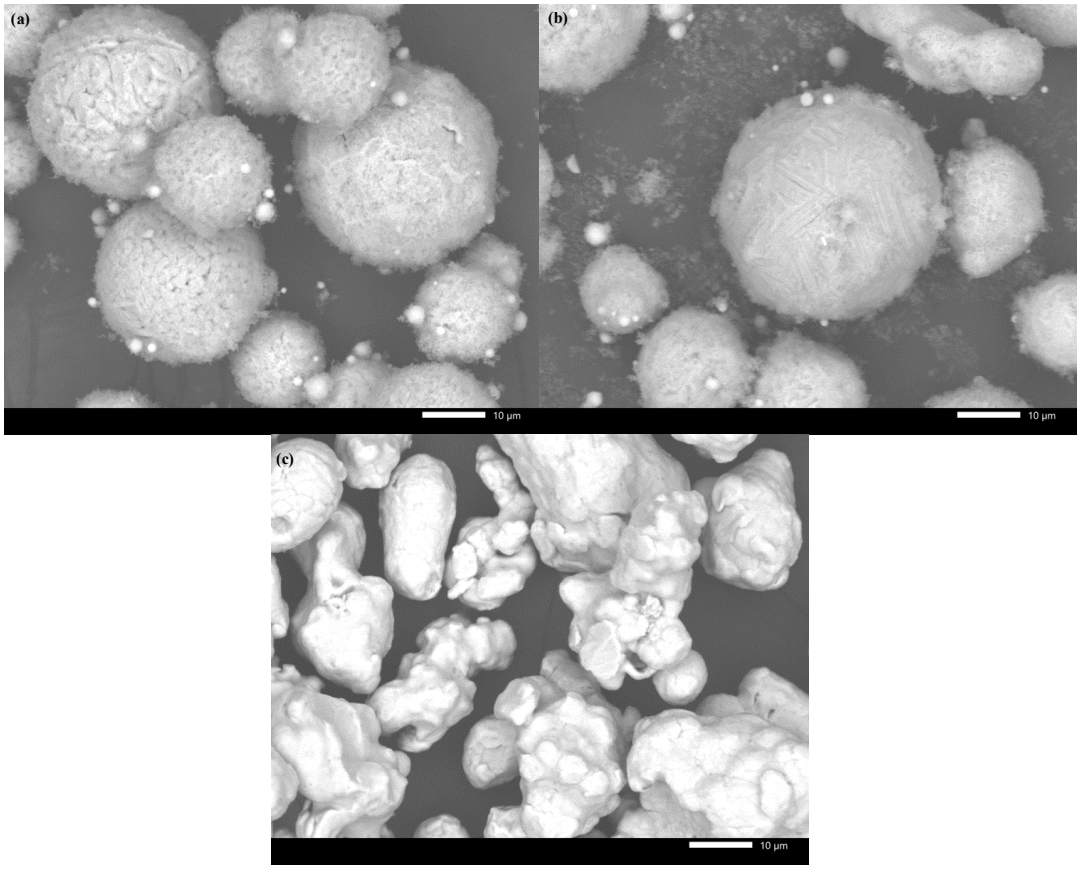

Figure 5. SEM-Images of iron powder α (a) after experiment DLR-002-002, (b) after experiment DLR-002-003, as well as (c) before combustion.

The high density of the iron caused difficulties with pneumatic transport. Depending on the test, up to 94% of the powder was scattered to the sides and not transported upwards at all; Table 3 shows the details.

Table 3. Material loss in experiment series DLR-002: Fuel mass flows, collected ash mass flows and resulting material losses for all experiments in series DLR-002.

Experiment	Fuel mass flow in kg/h	Cyclonic ash mash in kg/h	Ash proportion of fuel
DLR-002-001	4.650	0.287	6.2%
DLR-002-002	1.920	0.782	40.7%
DLR-002-003	1.280	0.351	27.4%

Due to this lateral dispersion, the ignition behaviour of iron powders with different diameters was investigated before continuing with the third series of experiments. The ignition of iron powder β, with

a diameter of 10 µm, occurred immediately after the iron powder was fed into the combustion chamber, resulting in a rapid flame. In the case of iron powder α (with a diameter of 30 µm), individual particles quickly became incandescent, but the formation of flames took significantly longer. Several local ignitions were observed, the frequency and area fraction of which increased over time, but all of them extinguished quickly. Successful ignition occurred when several local ignitions took place, distributed across the entire reactor cross-section. This sequence is shown in Figure 6. Some local ignitions were also caused by micro-explosions, which is probably the reason for the small particles visible in Figures 4 and 5.

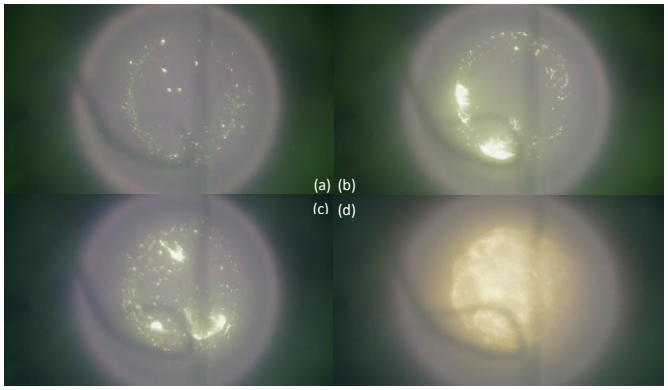

Figure 6. The ignition behaviour of powder α: (a) Several particles glow, but there is no flame. (b) Local ignitions occur, but they are quickly extinguished. (c) Several local ignitions occur simultaneously, covering a large part of the reactor cross-sectional area. (d) This leads to global ignition and thus to a flame.

The operating parameters of the further experiments (DLR-003 … 006) are summarized in Table 4. Experiment DLR-003 essentially covered the oxidation of powder β with an average diameter of 10 µm. Figure 7 shows the ignition process. The entire powder ignites in a single step; the rapid ignition of small particles contradicts the results of Ning et al. [1]. Presumably, the collective effect of heat generation outweighs other effects. However, this rapid ignition resulted in crust formation at the burner outlet within a few minutes, as shown in Figure 7. It is assumed that the high temperatures in the combustion chamber caused the iron powder to heat up in the burner, which promoted diffusion at contact points and thus led to sintering of particles. From the next experiment onwards, powder α was used again. The operating parameters of this experiment (DLR-004) are summarized in Table 4. Here, too, crust formation occurred within a few minutes. However, it was possible to record measured values here.

Figure 7. Experiment DLR-003: (left) Powder β ignites immediately after glowing. (right) A crust quickly formed, causing the burner to become clogged.

Figure 8 shows the temperatures measured at three different points in the combustion chamber (left) on the left and the fouling that occurred within 5 minutes (right). While the temperature in the afterburner and that of the flue gas remained approximately constant, the temperature in the combustion chamber rose sharply. According to the above argument, this would mean that hardly any fine particles are introduced into the afterburner chamber. Since rapid fouling occurred here, it is possible that the presence of fine particles promotes fouling at the burner outlet. Numerical and experimental work has shown [9-11] that the presence of fine particles in a particle bed can prevent its permeability. Although

the iron powder here was not in a particle bed, sintering also played a role and promoted this behaviour. There is evidence that freshly reduced fine iron powder particles can quickly form sintered cakes at 1000 °C [12]; a similar effect may have occurred here. Strong sintering was also observed during the oxidation of iron powder at low temperatures without flame formation, despite which complete oxidation of the powder was possible [13]. Alternatively, the sintering could be attributed to potentially incomplete cleaning. It is possible that after cleaning, traces of sintered iron remained in the burner tube, which acted as contact points for renewed sintering. Furthermore, it is also possible that after the experiment with 10 µm iron powder (powder β), residues of the powder remained in the combustion chamber, which acted as fine particles to trigger crust formation. In addition, the presence of these residues would have impaired heat transfer in the burner. It is currently unclear which of these explanations is correct. It cannot be ruled out that several mechanisms may have contributed to fouling.

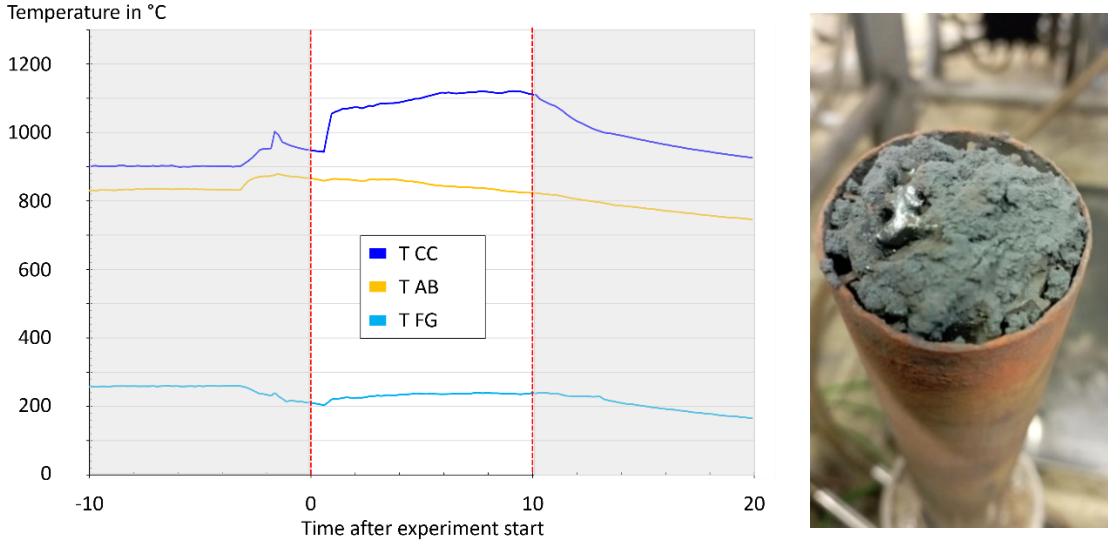

Figure 8. Experiment DLR-004: (left) Temperature curves over time at three different locations in the reactor: combustion chamber (CC), afterburner chamber (AB) and gas outlet (FG). (right) Fouling also occurred in this experiment.

In the subsequent experiment (DLR-005), only the target O_2 concentration in the flue gas was increased with the aim of increasing the volume flow through the reactor and thus improving particle transport through the reactor. The exact operating parameters can be found in Table 4. This was however only partially successful: although crust formation was delayed, the burner still became clogged after approximately 25 minutes.

Table 4. parameters of experiments DLR-003 … 006.

Experiment	T CC in °C	T AB in °C	Vol% O_2 in flue gas	Air volume flow in Nl/h	Fe mass flow in kg/h	Powder
DLR-003	800	800	10	-	-	β
DLR-004	1000	800	2.73	1634	3.90	α
DLR-005	1000	800	10	3283	3.28	α
DLR-006	800	800	10	3282	4.69	α

In the last experiment (DLR-006), the temperature of the combustion chamber was reduced to 800 °C to reduce crust formation. Further operating parameters are shown in Table 4. Although this measure could suppress crust formation for a while, it could not prevent it completely: after approx. 25 minutes, the experiment was stopped again.

The PSDs of the oxidized iron powder from both of these experiments are shown in Figure 9. In addition to the expected peak at 30 µm, many smaller peaks are visible. Most of these are probably

signs of smaller particles originating from explosions, as can be seen in Figures 4 and 5. The peaks at approx. 10 µm are interesting: these could be a sign of residues of powder β, which caused the fouling.

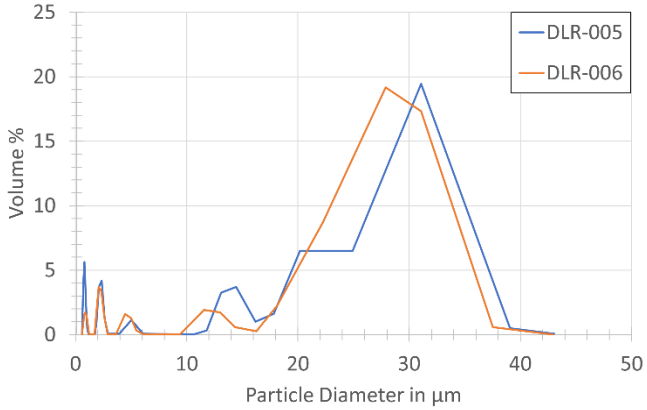

Figure 9. Particle size distribution of the oxidized powder from experiment series DLR-005 (blue) and DLR-006 (orange).

Images of the crust can be seen in Figure 10. The underside consists of a smooth and a rough section formed from layers. The upper side consists of dendritic areas that are clearly separated from each other. Small brown areas are visible on both sides, but the colour of the crust is predominantly grey. Oxidation on the surface during storage cannot be ruled out.

Figure 10. Images of the crust formation around the burner outlet: The top is shown on the left and the bottom on the right.

Summary and outlook

The Zittau Iron Combustion Chamber (ZIICC), a vertically aligned micro combustion chamber that replicates the combustion behaviour of industrial coal combustion chambers, was used for the first time to burn iron powder. After initially demonstrating the feasibility of iron powder combustion in such a combustion chamber, initial tests provided some process engineering data on the combustion process. In further tests, the problem of crust formation was observed, which occurred repeatedly despite different operating conditions. This could be due to the presence of tiny particles of around 2 µm in size, which became lodged between the larger particles and made sinter contact, as observed both numerically and experimentally. Alternatively, it could be the result of incomplete cleaning of the burner, leaving residues of sintered iron or small iron particles in the burner, which simultaneously acted as contact points and thermal insulation for new sintering processes. It is currently unclear which mechanism was actually at work, or whether several mechanisms played a role.

Next, REM images and particle size distributions of the powder leading to crust formation are generated and analysed to gain insights into this behaviour. It is also advisable to create a way of measuring the temperature in the burner tube. Further considerations relate to efforts to prevent crust formation. This would make it possible to install cooling at the bottom of the combustion chamber or an ash extraction system. However, it should be noted that industrial coal combustion chambers differ from the ZIICC in some respects, so the problem of crust formation may not exist there. Industrial combustion chambers often have a gas flow from bottom to top, but the burners are horizontal and not bottom burners. The gas flow rates and turbulent intensity are much higher in industrial combustion chambers. Both could prevent fouling from occurring in industrial combustion chambers. It is likely that

small particles are transported well with the main flow but burned quickly, while larger particles are transported poorly but have better ignition properties. All these points suggest that industrial iron combustion in converted combustion chambers remains a desirable goal, and that the obstacles presented in this article can certainly be overcome.

Acknowledgements
This work was carried out as part of the DLR project 'IronCircle®' and the cluster project 'Clean Circles'.

Literature

[1] Ning D., Li Y., Li T., Böhm B., Dreizler .: *Size-resolved ignition temperatures of isolated iron microparticles*, Combustion and Flame, 270, 11379, 2024.
[2] Deutschmann M. P., Sperling A., et al.: *Single iron particle combustion - A morphology study of partially oxidized iron particles*, Powder Technology, 445, 120102, 2024.
[3] Goroshin S., Tang F.-D., Higgins A. J., Lee J. H. S.: *Laminar dust flames in a reduced-gravity environment*, Acta Astronautica, 68, 656-666, 2011.
[4] Fedoryk M., Stelzner B., Harth S., Trimis D.: *Experimental investigation of the laminar burning velocity of iron-air flames in a tube burner*, Applications in Energy and Combustion Science, 13, 100111, 2023.
[5] Baigmohammadi M., Prasidha W., et al.: *Towards utilization of iron powders for heating and power*, Applications in Energy and Combustion Science, 13, 100116, 2023.
[6] Prasidha W., Baigmohammadi M., Shoshin Y., de Goey, P.: *Towards an efficient metal energy carrier for zero–emission heating and power: Iron powder combustion*, Combustion and Flame, 268, 113655, 2024.
[7] Steffens P., Hebel J., et al.: *Exploring turbulent methane-assisted iron dust combustion: A combined experimental and numerical study of a 47 kW th lab-scale combustor*, Fuel, 392, 135205, 2025.
[8] Ilinich M., Zanganeh K., Shafeen A., Staneva K.: *Metal Fuel Combustion Tests Using NRCan's 0.3 MWth Vertical Combustor Research Facility*, ASME Turbo Expo 2024, London, UK, 2024.
[9] Takahashi H., Kawai H., Kondo T., Sugawara M.: *Permeation and Blockage of Fine Particles Transported by Updraft through a Packed Bed*, ISIJ International, 51, 1608-1616, 2011.
[10] Luo Z.G., Zhou H. et al.: *DEM study of blockage behaviour of cohesive fine particles in a packed structure of large particles*, Powder Technology, 314, 102-109, 2017.
[11] Fukuda M., Suziku J., Kawai H., Nohami H.: *Numerical Analysis on Passage and Blockage Behaviors of Fine Particles through an Orifice Consists of Coarse Particles*, ISIJ International, 55, 1291-1298, 2015.
[12] Walther G., Büttner T. et al.: *Properties and sintering behaviour of fine spherical iron powders produced by new hydrogen reduction process,* Powder Metallurgy, 57, 176-183, 2014.
[13] Fradet Q., Fong S., et al.: *Thermogravimetric and microstructural analysis of the low-temperature oxidation of iron powders*, Fuel, 401, 135866, 2025